

Article

First-Principles Study on Mechanical and Optical Behavior of Plutonium Oxide under Typical Structural Phases and Vacancy Defects

Jin-Xing Cheng ^{1,*}, Fei Yang ², Qing-Bo Wang ¹, Yuan-Yuan He ², Yi-Nuo Liu ², Zi-Yu Hu ^{2,*} , Wei-Wei Wen ¹, You-Peng Wu ¹, Cheng-Yin Zheng ¹, Ai Yu ¹, Xin Lu ¹ and Yue Zhang ¹

¹ Beijing Institute of High Technology, Beijing 100094, China

² College of Mathematics and Physics, Beijing University of Chemical Technology, Beijing 100029, China

* Correspondence: chengjx@tsinghua.org.cn (J.-X.C.); huziyu@mail.buct.edu.cn (Z.-Y.H.)

Abstract: The chemical corrosion aging of plutonium is a very important topic. It is easy to be corroded and produces oxidation products of various valence states because of its 5f electron orbit between local and non-local. On the one hand, the phase diagram of plutonium and oxygen is complex, so there is still not enough research on typical structural phases. On the other hand, most of the studies on plutonium oxide focus on PuO₂ and Pu₂O₃ with stoichiometric ratio, while the understanding of non-stoichiometric ratio, especially for Pu₂O_{3-x}, is not deep enough. Based on this, using the DFT + U theoretical scheme of density functional theory, we have systematically studied the structural stability, lattice parameters, electronic structure, mechanical and optical properties of six typical high temperature phases of β-Pu₂O₃, α-Pu₂O₃, γ-Pu₂O₃, PuO, α-PuO₂, γ-PuO₂. Further, the mechanical properties and optical behavior of Pu₂O_{3-x} under different oxygen vacancy concentrations are analyzed and discussed in detail. The result shows that the elasticity modulus of single crystal in mechanical properties is directly related to the oxygen/plutonium ratio and crystal system. As the number of oxygen vacancies increases, the mechanical constants continue to increase. In terms of optical properties, PuO has the best optical properties, and the light absorption rate decreases with the increase of oxygen vacancy concentration.

Keywords: plutonium oxides; density functional theory; numerical simulation; optical properties



Citation: Cheng, J.-X.; Yang, F.; Wang, Q.-B.; He, Y.-Y.; Liu, Y.-N.; Hu, Z.-Y.; Wen, W.-W.; Wu, Y.-P.; Zheng, C.-Y.; Yu, A.; et al. First-Principles Study on Mechanical and Optical Behavior of Plutonium Oxide under Typical Structural Phases and Vacancy Defects. *Materials* **2022**, *15*, 7785. <https://doi.org/10.3390/ma15217785>

Academic Editor: Wei Guo

Received: 12 October 2022

Accepted: 2 November 2022

Published: 4 November 2022

Publisher's Note: MDPI stays neutral with regard to jurisdictional claims in published maps and institutional affiliations.



Copyright: © 2022 by the authors. Licensee MDPI, Basel, Switzerland. This article is an open access article distributed under the terms and conditions of the Creative Commons Attribution (CC BY) license (<https://creativecommons.org/licenses/by/4.0/>).

1. Introduction

The study of plutonium and its oxides has received continuous attention due to the complexity of the 5f state localized local/discrete domain of plutonium (Pu), resulting in a complex and rich phase diagram of plutonium oxide [1–3]. Plutonium and its oxide are important components of mixed oxide fuel in fast breeder reactors and advanced heavy water reactors [4–11], which plays an important role in the nuclear industry. Of course, they may also be stored as radioactive waste for long periods [12]. The phase diagram of plutonium oxide is intricate by the presence of multiple suboxides. It is recognized that the initial oxidation of plutonium produces trivalent sesquioxides (Pu₂O₃), followed by the trivalent dioxides (PuO₂). The coexistence of PuO₂ and plutonium leads to a reduction reaction of 3PuO₂ + Pu → 2Pu₂O₃, which is feasible in thermodynamics and results in a Pu₂O₃/Pu interface. In plutonium oxide layer, other non-stoichiometric plutonium oxides PuO_{2-x} (0 < x < 0.5) can also be formed. The ratio of Pu₂O₃ to PuO₂ is very sensitive to temperature and other external environments [1,13–17]. Generally, the base state of plutonium suboxide is the hexagonal structure β-Pu₂O₃ (P3m1), in addition, there is another oxide with a body-centered cubic structure (α-PuO_{1.52}) [18]. Further studies revealed that the cubic phase sesquioxide-plutonium (α-Pu₂O₃) also exists stably. α-Pu₂O₃ consists of 32 plutonium atoms and 48 oxygen atoms (Ia-3 space group) but it has not been prepared as a single-phase compound. This is because α-Pu₂O could only be stable below

300 °C and can be partially reduced on PuO₂ by the mixture of PuO_{1.52} and PuO_{1.98} [19] at high temperature, and then cooled to room temperature. Above 650 °C, 18 low-valence oxides between PuO_{1.61} and PuO₂ (i.e., PuO_{1.61+y}) mainly exist in a single-phase structure and can be prepared by reducing PuO₂ to carbon or hydrogen in vacuum [19]. So far, their final structure of this phase has yet to be determined. However, above 650 °C, 18 low-valence oxides between PuO_{1.61} and PuO₂ (i.e., PuO_{1.61+y}) are likely to be the subchemometric plutonium dioxide (PuO₂) phase. Additionally, the structure of PuO_{1.61} is closely related to cubic PuO_{1.52}. Therefore, it can be preliminarily described as the same cubic structure with 32 metal atoms and 51/52 oxygen atoms in a single cell. In contrast, in XRD measurements above 300 °C, [19] only strong pseudo-face-centered cubic reflections can be observed. Above 650 °C, PuO₂ can survive in a super-poor oxygen state, where the oxygen stoichiometry ratio can be reduced to PuO_{1.7} or even PuO_{1.6} [20]. The presence of oxygen also confirmed from density measurements at 750 °C vacancies, rather than the formation of interstitial plutonium ions.

Theoretically, it is a challenge to study plutonium oxides within the framework of electronic structure calculation based on standard Density Functional Theory (DFT). Due to the narrow *f*-band, close proximity to *d* and *s* orbitals in the metallic element plutonium, the phenomena of significant dynamic charge rise and fall exhibit in metallic bonds [21–24]. In the standard framework of local density generalization and generalized gradient generalization, the local effect of *f*-electrons caused by strong electron-electron interaction is not captured. To overcome this difficulty, different methods such as calculations involving self-interaction corrections (SIC) [25,26], mixed exchange correlation functions [27,28] or intra-atomic Coulomb interactions (Hubbard's *U*-parameters) [29–33] have been proposed and applied to study the two stoichiometric oxides (PuO₂, Pu₂O₃) in terms of structural, electronic, thermodynamic and optical properties [34–36]. Raymond et al. [37] calculated the electronic properties of the native (11 $\bar{2}$ 0) surfaces of β -Pu₂O₃ and found that the anti-ferromagnetic structure was more stable than the ferromagnetic structure. Lu et al. [38] used DFT + *U* method to determine the stability of charged defects in PuO₂. Petit et al. [25] analyzed the electronic structures of PuO_{2.25}, PuO_{1.75} and PuO₂ using the SIC approximation. Agarwal et al. [39] used the Gibbs Free Energy Model to calculate the phase diagram of PuO_{2-x} (0 < *x* < 0.5) and observed the mixed-phase gap behavior of PuO₂ and PuO_{1.7}. The results showed that the pure up Pu-O system can reduce to 60% of the plutonium to the +3 oxidations state while maintaining the face-centered cubic (fcc) structure. However, there are still few studies on high-temperature phase stability, electronic structure and formation mechanism of non-chemiscale PuO₂ and Pu₂O₃, especially for typical high-temperature phases and Pu₂O_{3-x} (0 < *x* < 1) with different concentrations of oxygen vacancy defects. In this paper, the mechanical and optical properties of six typical high-temperature phase structures of Pu oxides are systematically discussed by DFT + *U* method, including β -Pu₂O₃, α -Pu₂O₃, γ -Pu₂O₃, PuO, α -PuO₂, γ -PuO₂. Considering the obvious influence of vacancy defects on the properties of the system [40], we have also focused on the mechanical and optical properties of β -Pu₂O₃, structures with different concentrations of oxygen vacancy defects.

2. Computational Methods

First-principles calculation is carried out using the VASP (Vienna ab initio simulation package) software package [41]. The generalized-gradient approximation (GGA) with Perdew-Burke-Emzerhof (PBE) form [42] was used to describe the exchange-correlation functional. Setting the cut-off energy as 540 eV, we take the 6s²7s²6p⁶6d²5f⁴ of plutonium and the 2s²2p⁴ electrons of O as valence electrons [43] to participate in the calculation. The in situ repulsive energy of the plutonium 5f orbital electrons is considered in the calculations, and the values of *U* and *J* are, respectively, 4.75 eV and 0.75 eV [44]. For the calculations of the β -Pu₂O₃, α -Pu₂O₃, γ -Pu₂O₃, PuO, α -PuO₂, and γ -PuO₂ and the Monkhorst-Pack k-point grid for the Brillouin zone integral were sampled on 10 × 10 × 6(β -Pu₂O₃), 7 × 7 × 7(α -Pu₂O₃), 10 × 10 × 7(γ -Pu₂O₃), 8 × 8 × 8(PuO),

$8 \times 8 \times 8(\alpha\text{-PuO}_2)$, $7 \times 7 \times 10(\gamma\text{-PuO}_2)$ [7]. All structures were completely relaxed and the residual force was less than $0.01 \text{ eV}/\text{\AA}$.

Spin-polarized are included in structural optimizations. Here, we consider three possibilities for the magnetic states: nonferromagnetic (NM), ferromagnetic (FM) and antiferromagnetic (AFM) for all the oxides, see Table S1. In the following FM calculations, we use the collinear 1-k structure where the atomic spin moment is along the [001] direction. Energy formation is the total energy of a crystal minus the energy of the individual atoms contained in the crystal. In order to analyze the structural stability of the six plutonium oxides, their energy formation (E_{form}) has been calculated,

$$E_{form} = [E_{tot}(\text{Pu}_m\text{O}_n) - mE_{tot}(\text{Pu}) - nE_{tot}(\text{O})]/(m+n) \quad (1)$$

where m and n are the number of Pu and O atoms in the supercell. Respectively, $E_{tot}(\text{Pu}_m\text{O}_n)$, $E_{tot}(\text{Pu})$ and $E_{tot}(\text{O})$ are the total energy of per atom in their solid state. In general, the lower the formation energy, the more stable the solid solution. Additionally, the lower the formation energy of impurities, the more efficient the doping process.

For the six plutonium oxides, three independent elastic stiffness constants C_{11} , C_{12} , C_{44} were calculated by Voigt Method and obtained the Bulk Modulus (B), Shear Modulus (G), Young's Modulus (E) and Poisson's Ratio (ν). It is calculated as follows:

$$B = \frac{1}{3} [C_{11} + 2C_{12}] \quad (2)$$

$$G = \frac{1}{5} [C_{11} - C_{12} + 3C_{44}] \quad (3)$$

$$E = \frac{9BG}{3B + G} \quad (4)$$

$$\nu = \frac{3B - 2G}{2(3B + G)} \quad (5)$$

Other than that, Debye temperature is also closely related to the elastic constant. Based on the estimation of the average speed of sound (v_m) in a given material, the commonly used method of calculating Debye temperature is as follows:

$$\theta_D = \frac{h}{k} \left[\frac{3n}{4\pi} \left(\frac{N_A \rho}{M} \right)^1 \right]^{\frac{1}{3}} v_m \quad (6)$$

As shown in the formula above, h , k , N_A , n , M and ρ represent Planck's Constant, Boltzmann's Constant, Avogadro's Number, the atoms, molecular weight and density of organic cations. The average sound velocity (v_m) can be calculated by shear velocity (v_t) and compression velocity (v_l), respectively. v_m is related to v_t and v_l and are listed as follows:

$$v_t = \sqrt{G/\rho} \quad (7)$$

$$v_l = \sqrt{\left(B + \frac{3}{4}G \right) / \rho} \quad (8)$$

$$v_m = \left[\frac{1}{3} \left(\frac{2}{v_l^3} + \frac{1}{v_t^3} \right) \right]^{-\frac{1}{3}} \quad (9)$$

The optical properties of a compound are described by a complex function. The imaginary part of the dielectric tensor is determined by the sum of the following empty band states:

$$\epsilon_2(\omega) = \frac{2\pi e^2}{V\epsilon_0} \sum_{k,v,c} \delta(E_k^c - E_k^v - \hbar\omega) |\langle \Psi_k^c | \mu \cdot r | \Psi_k^v \rangle|^2 \quad (10)$$

ϵ_0 is the vacuum dielectric constant, V is the crystal volume. v and c , respectively, denotes the valence and conduction bands. $\hbar\omega$ is the energy of the incident phonon. \mathbf{u} is defined as the vector of incident electric field polarization. $\mu \cdot \mathbf{r}$ is the momentum operator. Ψ_k^c and Ψ_k^v are the wave functions of point k the conduction and valence bands, respectively. The real part of the dielectric tensor is proposed by the well-known Kramers-Kronig relation:

$$\epsilon_1(\omega) = 1 + \frac{2}{\pi} P \sum_{k,v,c} \int_0^\infty \frac{\epsilon_2(\omega')\omega'}{\omega'^2 - \omega^2 + i\eta} d\omega' \quad (11)$$

3. Results and Discussion

3.1. Crystal Structure Analysis

Plutonium oxide has multiple structures, and Figure 1 shows the crystal structure parameters and local charge density of six plutonium oxides. Pu_2O_3 has three forms, with $\beta\text{-Pu}_2\text{O}_3$ containing in the tripartite crystal system (P3m1 space group), $\alpha\text{-Pu}_2\text{O}_3$ containing in the cubic crystal system (Pn3m space group) and $\gamma\text{-Pu}_2\text{O}_3$ containing in the tetragonal crystal system (P4m2 space group). PuO belongs to the cubic crystal system (Fm3m space group). The PuO_2 exists in two forms and $\alpha\text{-PuO}_2$ belongs to the cubic crystal system (Fm3m space group) and $\gamma\text{-PuO}_2$ belongs to the tetragonal crystal system (P42/mnm) space group. Through structural optimization, their equilibrium lattice constants were calculated and listed in Table 1.

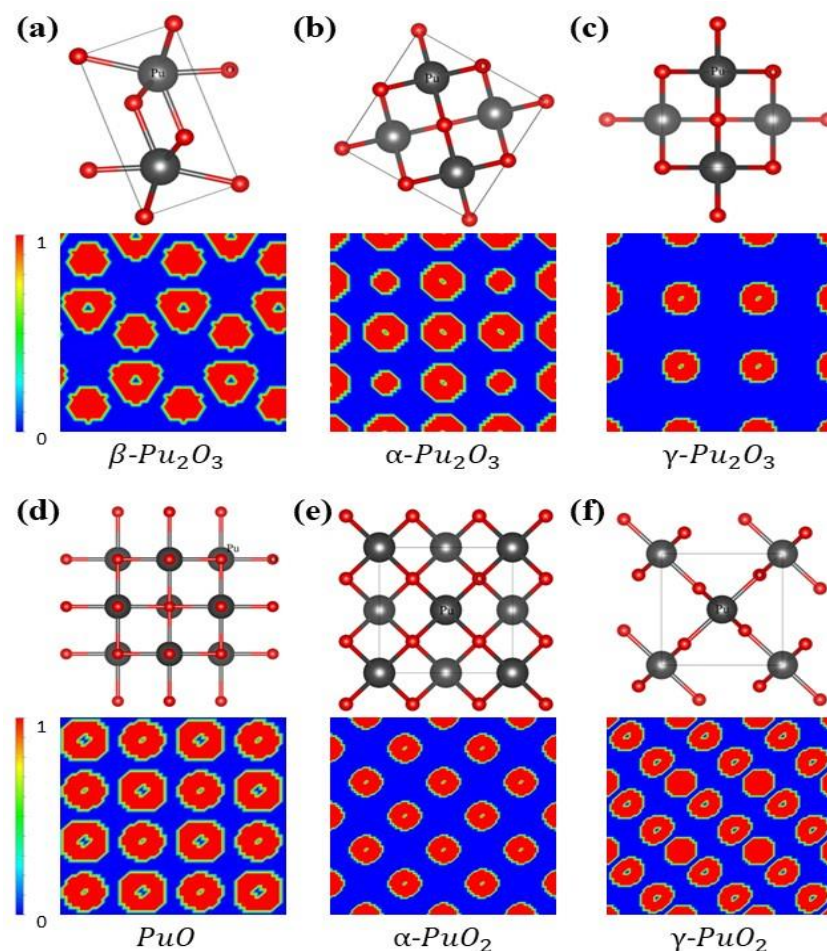


Figure 1. Optimized geometries of (a) $\beta\text{-Pu}_2\text{O}_3$, (b) $\alpha\text{-Pu}_2\text{O}_3$, (c) $\gamma\text{-Pu}_2\text{O}_3$, (d) PuO , (e) $\alpha\text{-PuO}_2$, (f) $\gamma\text{-PuO}_2$ are shown in the figure above. The gray atoms indicate the Pu atoms. The red atoms indicate O atoms. Their local electronic density states are also listed. Pu and O atoms are represented in blue and red color, respectively.

Table 1. Lattice parameters of β -Pu₂O₃, α -Pu₂O₃, γ -Pu₂O₃, PuO, α -PuO₂, γ -PuO₂, include formation energy, lattice constant and bond angle α , β , γ .

Plutonium Oxide	Formation Energy (eV)	a (Å)	b (Å)	c (Å)	α (°)	β (°)	γ (°)
β -Pu ₂ O ₃	-3.411	3.76	3.76	5.97	90	90	120
α -Pu ₂ O ₃	-3.357	5.38	5.38	5.38	90	90	90
γ -Pu ₂ O ₃	-3.401	3.76	3.76	5.97	90	90	120
PuO	-2.808	4.97	4.97	4.97	90	90	90
α -PuO ₂	-3.673	3.76	3.76	5.97	90	90	120
γ -PuO ₂	-3.507	3.76	3.76	5.97	90	90	120

The formation energies of the six oxides were calculated according to Equation (1). As shown in Table 1, the formation energies of all six plutonium oxides are negative, which indicates that the formation of the compounds is exothermic. β -Pu₂O₃ and γ -Pu₂O₃ have the same lattice constants a, b, c and bond angles α , β , γ , but β -Pu₂O₃ has a lower formation energy. β -Pu₂O₃ structure is more energetically stable than γ -Pu₂O₃. By comparison, the formation energies of the two PuO₂ structures show that the α -PuO₂ structure is more stable than the γ -PuO₂ structure.

3.2. Band Structure and Density of Electronic States

As shown in Figure 2, we have calculated the energy band diagrams and total electron density of states (TDOS) diagrams to investigate the properties of the six plutonium oxides. Based on the properties of plutonium, spin orbit coupling is considered in our calculations. From Figure 2a–f, we can see that electrons with the same spin state are concentrated near the Fermi energy level, and at energies below -2 eV. The TDOS is contributed by both spin-up and spin-down electrons, and at energies -2 eV $<$ E $<$ 2 eV, β -Pu₂O₃ and α -PuO₂ is only contributed by spin up states in -2 eV to 2 eV, but with little effect of the spin-down electronic states for β -Pu₂O₃ and α -PuO₂ in -2 eV to 2 eV. Additionally, at energies greater than 2 eV, the TDOS is mainly contributed by spin-down electrons. In view of this, we can filter the electrons with different spin states according to different energy ranges, which is of great importance for quantum applications.

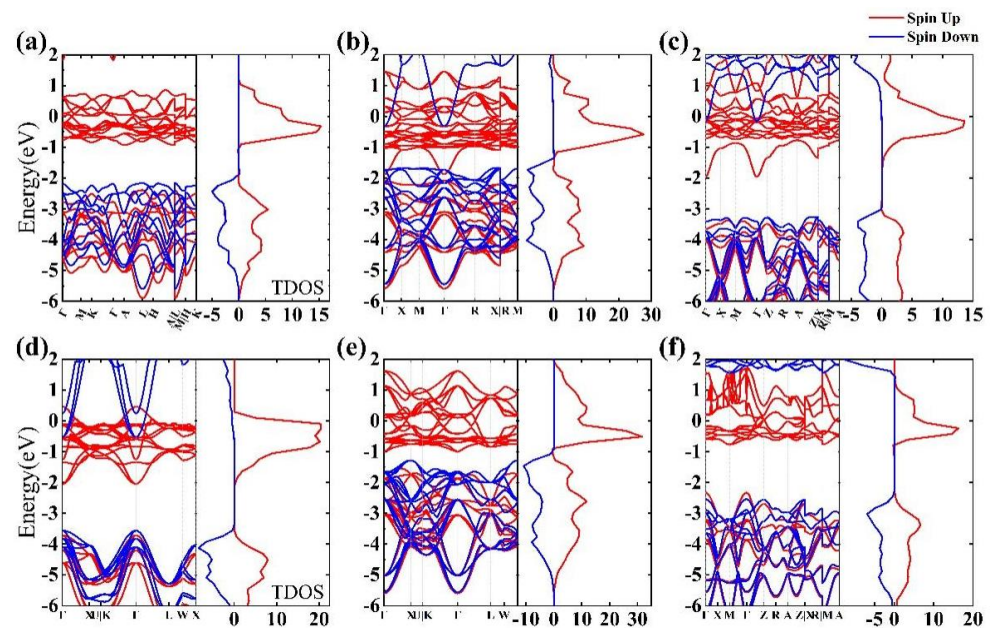


Figure 2. The upper left figure shows the electronic structure band, and the upper right figure shows the total electron density of states (TDOS) of (a) β -Pu₂O₃, (b) α -Pu₂O₃, (c) γ -Pu₂O₃, (d) PuO, (e) α -PuO₂, (f) γ -PuO₂. The red line is represented by electrons that spin downwards and the blue line is represented by electrons that spin upwards. The location with an energy of 0 represents the Fermi level.

In general, the stability of the material structure was determined by the position of the value of the electronic density of states (DOS) at the Fermi energy level. For the metallic system, the distribution of electronic DOS will span the Fermi level and have a great impact on the properties of materials. In Figure 2, the red line indicates spin up, and the blue line indicates spin down. We can see that the spin up electron density of the six plutonium oxides crosses the Fermi level. However, only the electron densities of Figure 2b–d cross the Fermi level for spin down electrons, while for spin down electrons, the band gaps of Figure 2a,e,f are 4.46 eV, 4.85 eV and 4.11 eV. We have calculated the electronic projected density of states (PDOS) of plutonium oxides, as shown in Figure 3. It shows that the overall picture is similar and the electron contribution to the density of states can be discussed in three intervals from Figure 3a–f. At energies below -1 eV, for β -Pu₂O₃, α -Pu₂O₃, α -PuO₂ and γ -PuO₂, the DOS is mainly contributed by the p-orbitals of the oxygen atom, while the orbital contributions of γ -Pu₂O₃ and PuO are similar. Near the Fermi energy level, it can be clearly seen that the f-orbiting electrons of the plutonium atom play a major role and are contributed by the separate spin-up electron. We believe that for the six plutonium oxides, the f-orbital electrons of Pu atom mainly contribute to the DOS at the Fermi level. The contribution of O atom is small, because the energy of 2p electron in the outermost layer of oxygen atom is smaller than 5f of Pu. At the same time, the 2p orbital electron of oxygen atom has a large expansibility which means the degree of electron dispersion is strong. From each figure, we can see an obvious spike in electronic density of states, which is mainly caused by the strong localization of 5f orbital electrons of Pu atom.

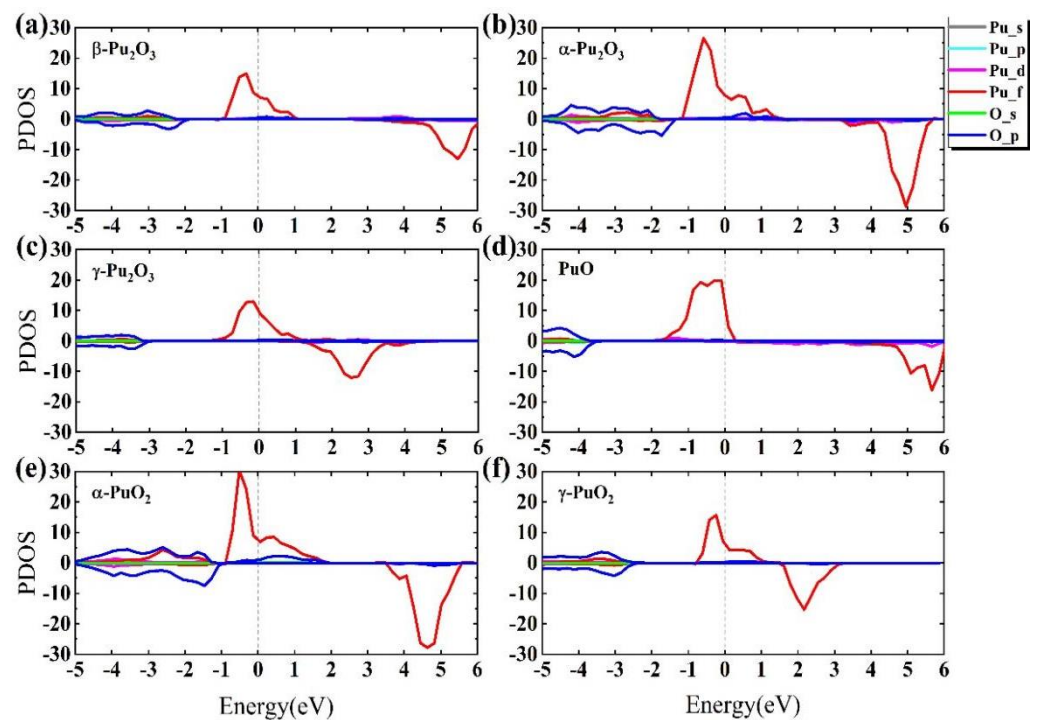


Figure 3. The electronic projected density of states (PDOS) of (a) β -Pu₂O₃, (b) α -Pu₂O₃, (c) γ -Pu₂O₃, (d) PuO, (e) α -PuO₂, (f) γ -PuO₂.

3.3. Mechanical and Optical Properties

Table 2 shows the mechanical constants C_{ij} of plutonium oxides. For a mechanically stable material with a cubic structure [45,46], the independent elastic constants need to meet the following three criteria $C_{11} > |C_{12}|$, $C_{44} > 0$ and $C_{11} + 2C_{12} > 0$. The Bulk modulus (B), Young's modulus (E), Shear modulus (G) and Poisson's ratio (ν) of several plutonium oxides are given in Table 3. Brittleness and ductility can be determined by the value of B/G. When B/G is small, the material is brittle; otherwise, it is ductile. From the calculations, it is possible to see that the B/G value of β -Pu₂O₃ is large and ductile. The bulk modulus (B)

indicates incompressibility, and Table 3 shows that PuO has the greatest incompressibility followed by α -PuO₂. The modulus of elasticity E is an important parameter to characterize material stiffness, which mainly reflects compressive strength of the material. From Table 3, we find that α -PuO₂ has the highest stiffness. The Shear modulus (G) is a measure of the ability of a material to resist shear deformation, and Table 3 shows that α -PuO₂ has the largest Shear modulus, so it has the strongest shear deformation resistance. In addition, the smaller Poisson's ratio is, the more brittle the material is. The result is consistent with our analysis above.

Table 2. Values of mechanical constants C_{ij} of each lead oxide.

	C_{11}	C_{12}	C_{13}	C_{14}	C_{33}	C_{44}	C_{66}
β -Pu ₂ O ₃	253.275	122.725	151.414	8.55	228.163	-8.55	65.275
α -Pu ₂ O ₃	305.341	4.798	4.798	-	305.341	-17.313	-17.313
γ -Pu ₂ O ₃	226.968	127.209	92.974	-	259.606	54.821	96.290
PuO	425.817	112.785	112.785	-	425.817	45.283	45.283
α -PuO ₂	3925.219	2276.845	2276.845	-	3925.219	65.254	65.254
γ -PuO ₂	4966.565	5302.567	112.485	-	572.217	-433.486	445.562

Table 3. Values of the Young's modulus (E), Bulk modulus (B) and Shear modulus (G) (in GPa), and Poisson's ratio (ν) of each plutonium oxide.

Plutonium Oxide	Bulk Modulus (GPa)	Young's Modulus (GPa)	Shear Modulus (GPa)	Poisson's Ratio
β -Pu ₂ O ₃	176.2	155.78	57.58	0.35
α -Pu ₂ O ₃	104.98	128.82	49.72	0.3
γ -Pu ₂ O ₃	148.87	171.67	65.63	0.31
PuO	217.13	205.43	76.52	0.34
α -PuO ₂	209.49	281.5	110.3	0.28
γ -PuO ₂	175.13	153.61	56.73	0.35

The study of optical properties of materials is one of the most effective techniques for analyzing various physical properties related to the electronic structure of materials. The dielectric function, optical absorption spectrum and reflection spectrum of plutonium oxide have been calculated and analyzed. The imaginary and real parts of the dielectric functions of plutonium oxide with different structures are shown in Figure 4. In the low energy region, the real part of the dielectric function decreases to low value with the energy increasing and then increases slowly and then remains essentially constant. The imaginary part of the dielectric function decreases as the energy increases in low energy region, a new peak at energies above 20 eV, but the peak decreases. The curve for PuO is the most unusual, with a unique peak in the low energy band. The absorption and reflection spectra of different structures of plutonium oxide are shown in Figure 4c,d. It shows that the photon absorption of plutonium oxides diminishes with the increasing wavelength. In the visible range, the absorption decreases and then increases steadily with the increasing wavelength. In the UV region, it shows that the different plutonium oxides have different peaks of wavelength absorption. Compared with other plutonium oxides, the absorption of some photons in the violet and UV regions is the strongest for PuO and forms the two highest peaks evident, with the plutonium oxides reflecting more significantly in the visible region and stable in the infrared region as the wavelength increases. PuO remains the most unusual, with two distinct peaks. In Figure 4, the un-reported metastable oxide of α -Pu₂O₃ presents the highest dielectric properties. Light absorption spectra or reflection spectra also present different absorbed properties.

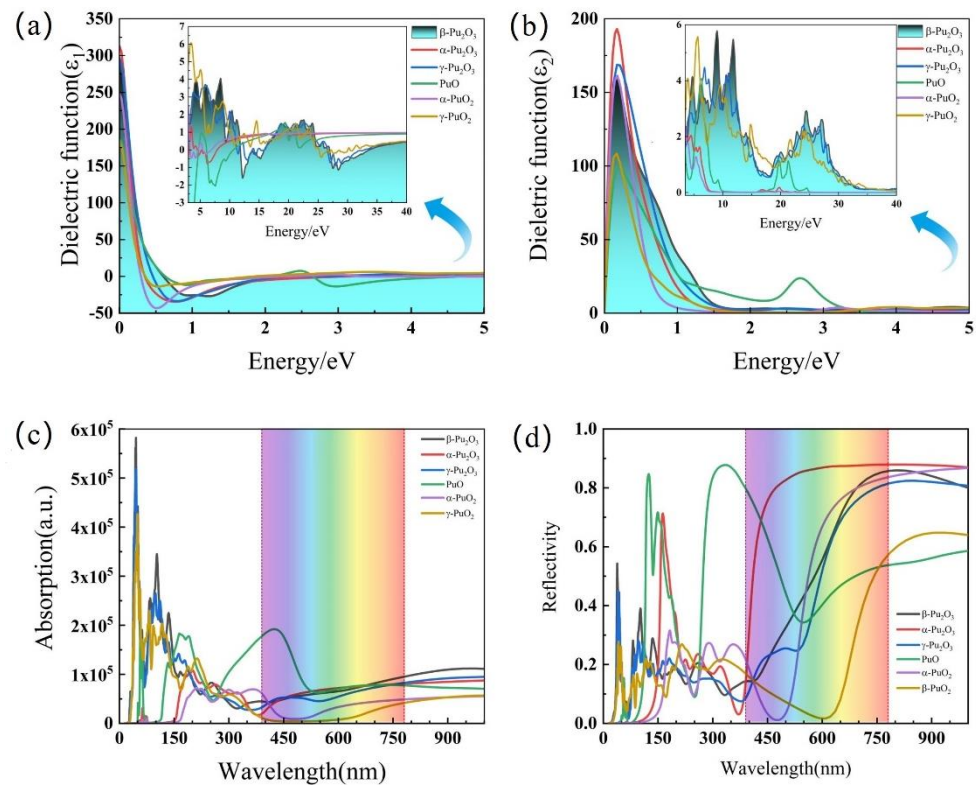


Figure 4. Real $\epsilon_1(\omega)$, imaginary $\epsilon_2(\omega)$ components of the dielectric function in (a,b). (c) shows light absorption spectra and (d) shows reflection spectra of studied oxide.

3.4. Mechanical and Optical Properties at Different Oxygen Vacancy Concentrations

After analyzing the previous research, we found that β -Pu₂O₃ is the most stable among the six plutonium oxides structures, and at the same time its moldability and forgeability are better. This is more meaningful and valuable for the research. The current research on plutonium oxides mainly focuses on PuO and PuO₂, but there are few studies on Pu₂O₃ under high temperature phase. So, we expanded the cell of β -Pu₂O₃ by $2 \times 2 \times 2$ times along the crystal direction to obtain the structure of β -Pu₁₆O₂₄. We studied the properties under different oxygen vacancy concentrations after rounding off its oxygen atoms in the ratio of 1:2:4:6 and obtained the electronic PDOS maps for (a) β -Pu₁₆O₂₃, (b) β -Pu₁₆O₂₂, (c) β -Pu₁₆O₂₀ and (d) β -Pu₁₆O₁₈. The above is shown in Figure 5. In the energy region below -4 eV, it is mainly the p orbitals of O atoms that contribute to the major DOS, followed by the d and f orbitals and p orbitals of Pu atoms. There are no electronic states that are occupied between energies -4 eV and -1 eV. As the energy continues to 0 eV, DOS is mainly influenced by f -orbitals of Pu atom, followed by d orbitals of Pu atom, and there is almost no contribution from the oxygen atom. Secondly, the contribution of the f orbitals of Pu to the DOS decreases as the oxygen vacancy concentration increases.

Debye temperature is an important physical quantity that reflects the interatomic bonding forces. The melting point of a material is positively correlated with the interatomic bonding force. The Debye temperature increases with the values of Pu/O increasing; when the value of Pu/O varies from 0.696 to 0.727, and decreases with the values of Pu/O increasing. When it varies from 0.727 to 0.889, β -Pu₁₆O₂₂ has the strongest interatomic bonding and the highest Debye temperature among the four calculated oxygen vacancy plutonium oxide structures. The crystal structure is more complex, the anharmonic degree of lattice vibrations is greater. If the lattice wave scattering is larger, the mean free path of phonons is smaller, and the thermal conductivity is lower. Results show that the lattice thermal conductivity of β -Pu₁₆O₂₃ is the lowest among the four oxygen vacancy plutonium oxides, as shown in Table 4.

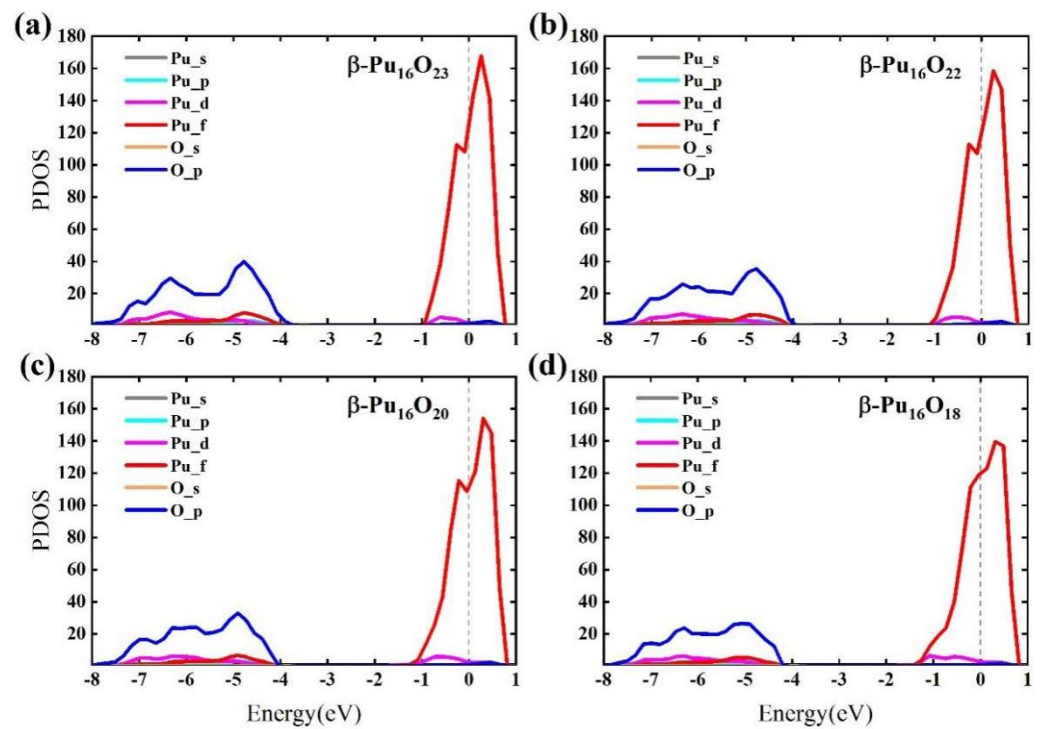


Figure 5. The electronic Pre-Departure Orientation Seminar (PDOS) of (a) β -Pu₁₆O₂₃, (b) β -Pu₁₆O₂₂, (c) β -Pu₁₆O₂₀, (d) β -Pu₁₆O₁₈.

Table 4. Values of the Debye temperature and lattice thermal conductivity of the studied structures.

Plutonium Oxide	Debye Temperature (K)	Lattice Thermal Conductivity
β -Pu ₁₆ O ₂₃	285.864	0.8124
β -Pu ₁₆ O ₂₂	307.852	0.8501
β -Pu ₁₆ O ₂₀	303.668	0.8250
β -Pu ₁₆ O ₁₈	301.879	0.8535

To further investigate the properties of β -Pu₂O₃ at different oxygen vacancy concentrations, we calculated the transverse sound velocity (v_t), longitudinal sound velocity (v_l) and average sound velocity (v_m) of Pu₁₆O₂₃, Pu₁₆O₂₂, Pu₁₆O₂₀ and Pu₁₆O₁₈. The result is shown in Figure 6a. The calculated Bulk modulus (B), Shear modulus (G), Young's modulus (E) and Poisson's ratio (ν) were compared with the elastic constants of Pu₃₂O₆₂, Pu₃₂O₆₀, Pu₃₂O₅₆ and Pu₃₂O₅₂ calculated by Ghosh et al. [47], which is shown in Figure 6b. We found that Pu₁₆O₂₀ is more special and manifested mechanical constants of $C_{11} > C_{33}$, $C_{66} > C_{44}$, while the values of C_{11} , C_{33} , C_{66} , C_{44} kept increasing as the number of oxygen vacancies of the other three oxides increases, which it always shows $C_{11} < C_{33}$, $C_{66} < C_{44}$. Comparing with the values of C_{ij} calculated by Ghosh et al. [47], who studied four plutonium oxides and found that the values of C_{11} , C_{33} , C_{44} , and C_{66} decrease gradually as oxygen vacancies increase. From Figure 6a, it shows that the transverse sound velocity (v_t), longitudinal sound velocity (v_l) and mean sound velocity (v_m) increase with the values of Pu/O increasing when the value of Pu/O varies from 0.696 to 0.727. They decrease with the values of Pu/O increasing when the value of Pu/O varies from 0.727 to 0.889. Shear modulus (G) is the ratio of shear stress to shear strain, which represents the ability of materials to resist shear strain. If the modulus is larger, the material is harder. The ratio of G to B (G/B) indicates the brittleness and toughness of material, and it can be found that Pu₁₆O₂₀ has the best brittleness and toughness of the four plutonium oxides we studied, while Pu₁₆O₂₃ has the smallest G/B value. That means the brittleness and toughness of the material gradually increases as the value of Pu/O increases from 0.696 to 0.8, and is

predicted to decrease when the values are greater than 0.8. It can be observed that Poisson's ratio (ν) gradually decreases as the value of Pu/O gradually increases from 0.69 to 0.8 and then gradually increases again when the values are greater than 0.8. Compared with the case calculated by Ghosh et al. [47], the study reveals that the oxygen vacancy profile of β -Pu₁₆O₂₄ does not vary in a single way.

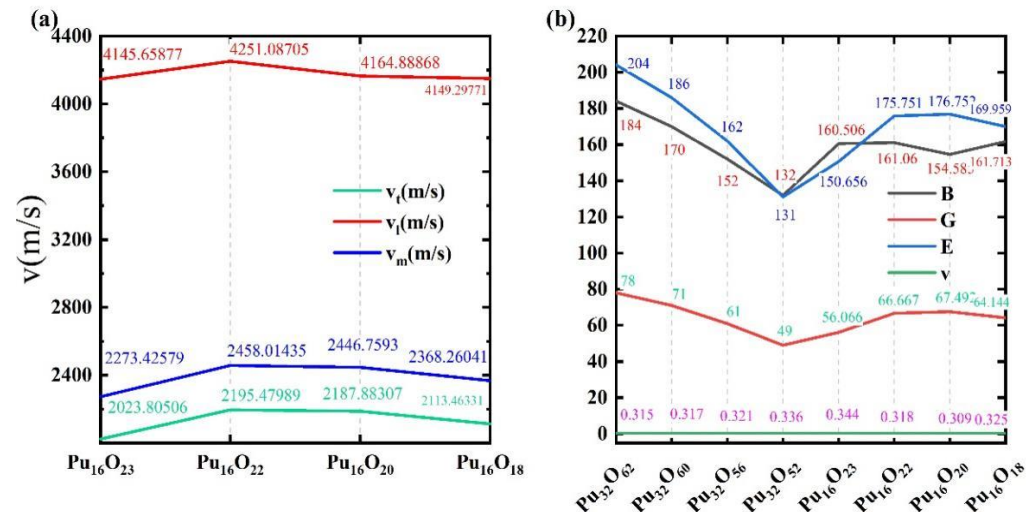


Figure 6. (a) Values of average sound velocity (v_m), longitudinal wave velocity (v_l), shear wave velocity (v_t) of Pu₁₆O₂₃, Pu₁₆O₂₂, Pu₁₆O₂₀, Pu₁₆O₁₈ using VASP. (b) Values of the Young's modulus (E), Bulk modulus (B) and Shear modulus (G) (in GPa), and Poisson's ratio (ν) of Pu₁₆O₂₃, Pu₁₆O₂₂, Pu₁₆O₂₀, Pu₁₆O₁₈ are compared with the values of Pu₃₂O₆₂, Pu₃₂O₆₀, Pu₃₂O₅₆, Pu₃₂O₅₂ calculated by Ghosh [47,48].

The imaginary and real parts of dielectric function of plutonium oxide at different oxygen vacancy concentrations are shown in Figure 7a,b. In the low energy region, the values of both real and imaginary parts of the dielectric function decrease. As oxygen atoms decrease, the energy gradually increases. The values of the real and imaginary parts of the dielectric function increase as oxygen atoms decrease. Figure 7c shows the optical absorption spectrum of plutonium oxide at different oxygen vacancy concentrations. The main absorption peak is around 40 nm (in the vacuum UV region), which indicates that most electrons can transition from the valence band to the conduction band by absorbing a small amount of energy corresponding to the system band gap. When the wavelengths are less than 700 nm, the absorption of light of the plutonium oxide increases with the decreasing numbers of oxygen atoms at the same wavelength of incident light. When a turnaround is near 700 nm, the absorption of the light of the plutonium oxide decreases with the decrease of oxygen atoms. Figure 7d shows the reflection spectrum of plutonium oxide at different oxygen vacancies. The reflection values are larger in the visible region from 380–790 nm. It shows that when the wavelengths are less than 700 nm, at the same wavelength, the light absorption of plutonium oxide increases with the decrease of oxygen atoms. However, there is a turnaround and the light absorption of plutonium oxide decreases as oxygen atoms decrease when wavelengths are around 700 nm. The change in the negative dielectric function is well supported the conclusions obtained in optical absorption spectrum and absorption spectrum.

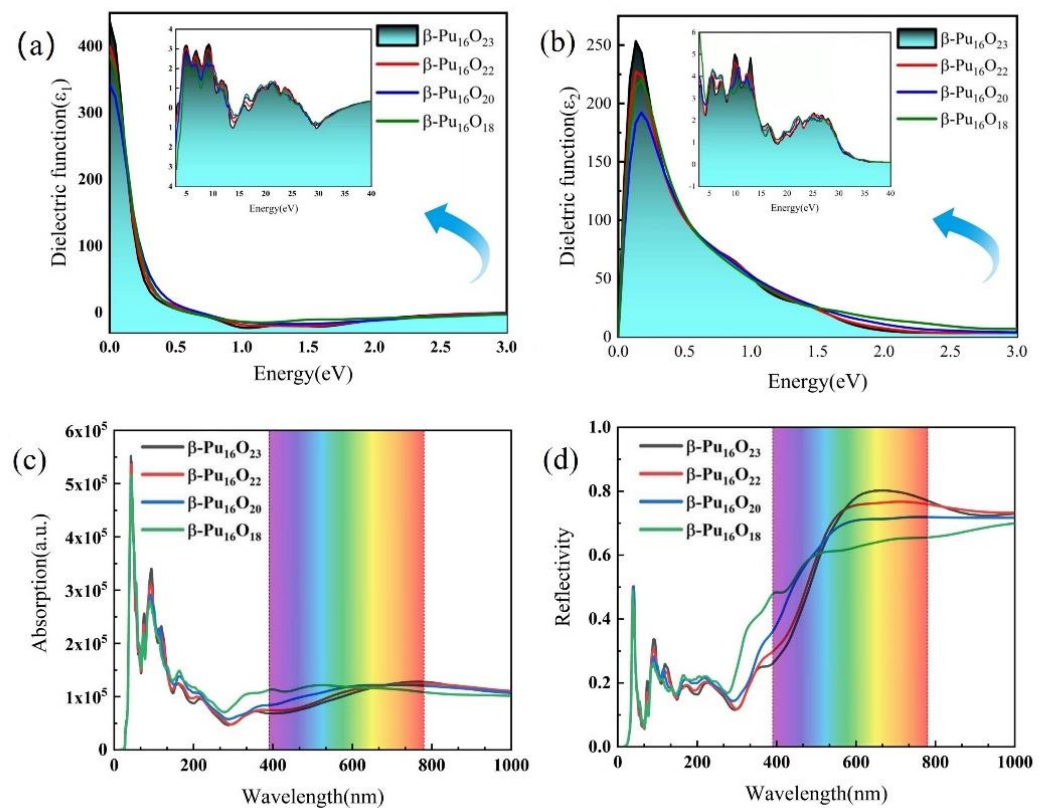


Figure 7. Real $\epsilon_1(\omega)$, imaginary $\epsilon_2(\omega)$ components of the dielectric function, light absorption spectra and reflection spectra of β -Pu₁₆O₂₃, β -Pu₁₆O₂₂, β -Pu₁₆O₂₀ and β -Pu₁₆O₁₈. (a) Real part of dielectric function. (b) Imaginary part of dielectric function. (c) Absorption spectra. (d) Reflection spectra.

4. Conclusions

After systematically investigating the electronic structure, mechanical and optical properties of plutonium oxides β -Pu₂O₃, α -Pu₂O₃, γ -Pu₂O₃, PuO, α -PuO₂, γ -PuO₂ and β -Pu₂O_{3-x} at different oxygen vacancy concentrations by using the first principles, the results show that the vicinity of the Fermi energy level is mainly determined by the spin-up electron state of 5f orbital of Pu atom, while the spin-down electronic states of the 5f orbitals are at higher energy levels. This is useful for distinguishing and screening the electrons of different spin states. The higher the oxygen/plutonium ratio, the greater the bonding between the crystalline atoms. The elastic modulus is higher, the material is harder. When the oxygen/plutonium ratio is 1.5, the elastic modulus of the γ crystal system is higher than β crystal system. The α crystal system is the smallest. However, at an oxygen/plutonium ratio of 2, the elastic modulus of α crystal system is higher than γ crystal system. For the study of the UV light of any of the plutonium oxides, PuO has the strongest absorption in the UV region and the most unusual reflective properties, which there are two reflective peaks in the entire waveband.

Supplementary Materials: The following supporting information can be downloaded at: <https://www.mdpi.com/article/10.3390/ma15217785/s1>.

Author Contributions: J.-X.C., Y.Z. and Z.-Y.H. initiated the project; J.-X.C., F.Y., Q.-B.W., Y.-Y.H. and Y.-N.L. performed calculations; W.-W.W., Y.-P.W., C.-Y.Z., A.Y. and X.L. supervised the project; J.-X.C., Z.-Y.H. and Y.Z. wrote the paper. All authors have read and agreed to the published version of the manuscript.

Funding: This work was financially supported by the National Natural Science Foundation of China (Grant No. 11604008, 11904027). We also acknowledge the computational support of computers at Tianhe2-JK in the Beijing Computational Science Research Center.

Institutional Review Board Statement: Not applicable.

Informed Consent Statement: Not applicable.

Data Availability Statement: The data presented in this study are available on request from the corresponding authors.

Conflicts of Interest: There are no conflict to declare.

References

1. Li, Q.; Lu, H. Structure and Thermodynamic Stability of $\text{PuC}_2(\text{g})$ Molecules. *Chin. J. Chem. Phys.* **2003**, *16*, 368–370. Available online: <http://cjcp.ustc.edu.cn/hxwlb/en/article/doi/10.1088/1674-0068/16/5/368-370> (accessed on 12 October 2022).
2. Butterfield, M.T.; Durakiewicz, T.; Guziewicz, E.; Joyce, J.J.; Arko, A.J.; Graham, K.S.; Moore, D.P.; Morales, L.A. Photoemission of surface oxides and hydrides of delta plutonium. *Surf. Sci.* **2004**, *571*, 74–82. Available online: <https://www.sciencedirect.com/science/article/pii/S0039602804010404> (accessed on 12 October 2022). [CrossRef]
3. Chikalla, T.D.; McNeilly, C.E.; Skavdahl, R.E. The plutonium-oxygen system. *J. Nucl. Mater.* **1964**, *12*, 131–141. Available online: <https://www.sciencedirect.com/science/article/pii/0022311564901321> (accessed on 12 October 2022). [CrossRef]
4. Chen, J.; Meng, D.Q.; Du, J.G.; Jiang, G.; Gao, T.; Zhu, Z.H. Molecular structure and spectroscopic study of plutonium oxides. *Acta Phys. Sin. (Chin. Ed.)* **2010**, *59*, 1658. [CrossRef]
5. Ghosh, P.S.; Somayajulu, P.S.; Arya, A.; Dey, G.K.; Dutta, B.K. Thermal expansion and thermal conductivity of $(\text{Th,Ce})\text{O}_2$ mixed oxides: A molecular dynamics and experimental study. *J. Alloys Compd.* **2015**, *638*, 172–181. Available online: <https://www.sciencedirect.com/science/article/pii/S0925838815007653> (accessed on 12 October 2022). [CrossRef]
6. Ghosh, P.S.; Somayajulu, P.S.; Krishnan, K.; Pathak, N.; Arya, A.; Dey, G.K. Thermal expansion and thermal conductivity of $(\text{Th,U})\text{O}_2$ mixed oxides: A molecular dynamics and experimental study. *J. Alloys Compd.* **2015**, *650*, 165–177. Available online: <https://www.sciencedirect.com/science/article/pii/S0925838815306587> (accessed on 12 October 2022). [CrossRef]
7. Ghosh, P.S.; Kuganathan, N.; Galvin, C.O.T.; Arya, A.; Dey, G.K.; Dutta, B.K.; Grimes, R.W. Melting behavior of $(\text{Th,U})\text{O}_2$ and $(\text{Th,Pu})\text{O}_2$ mixed oxides. *J. Nucl. Mater.* **2016**, *479*, 112–122. Available online: <https://www.sciencedirect.com/science/article/pii/S0022311516302884> (accessed on 12 October 2022). [CrossRef]
8. Ghosh, P.S.; Arya, A.; Dey, G.K.; Kuganathan, N.; Grimes, R.W. A computational study on the superionic behaviour of ThO_2 . *Phys. Chem. Chem. Phys.* **2016**, *18*, 31494–31504. [CrossRef]
9. Somayajulu, P.S.; Ghosh, P.S.; Arya, A.; Devi, K.V.V.; Sathe, D.B.; Banerjee, J.; Dutta, B.K. Thermal expansion and thermal conductivity of $(\text{Th,Pu})\text{O}_2$ mixed oxides: A molecular dynamics and experimental study. *J. Alloys Compd.* **2016**, *664*, 291–303. Available online: <https://www.sciencedirect.com/science/article/pii/S092583881532034X> (accessed on 12 October 2022). [CrossRef]
10. Somayajulu, P.S.; Ghosh, P.S.; Banerjee, J.; Babu, K.L.N.C.; Danny, K.M.; Mandal, B.P.; Mahata, T.; Sengupta, P.; Sali, S.K.; Arya, A. Experimental and molecular dynamics study of thermo-physical and transport properties of ThO_2 -5wt.% CeO_2 mixed oxides. *J. Nucl. Mater.* **2015**, *467*, 644–659. Available online: <https://www.sciencedirect.com/science/article/pii/S0022311515302993> (accessed on 12 October 2022). [CrossRef]
11. Shi, J.; Li, G.; Wan, L.; Gao, T.; Luo, W. New insights into the interfacial interactions of O_2 and H_2O molecules with PuH_2 (110) and (111) surfaces from first-principles calculations. *Int. J. Hydrog. Energy.* **2022**. Available online: <https://www.sciencedirect.com/science/article/pii/S036031992203823X> (accessed on 12 October 2022).
12. Meng, D.Q.; Jiang, G.; Liu, X.L.; Luo, D.L.; Zhang, W.X.; Zhu, Z.H. Structure and potential function of Pu_3 system. *Acta Phys. Sin. (Chin. Ed.)* **2001**, *50*, 1268. [CrossRef]
13. Alexandrov, V.; Shvareva, T.Y.; Hayun, S.; Asta, M.; Navrotsky, A. Actinide Dioxides in Water: Interactions at the Interface. *J. Phys. Chem. Lett.* **2011**, *2*, 3130–3134. [CrossRef]
14. Eloirdi, R.; Gouder, T.; Wastin, F.; Huber, F.; Shick, A.B.; Kolorenč, J. Dilution effect on the U 5f states in Au matrix: A photoemission spectroscopy study. *Phys. Rev. B* **2011**, *84*, 235143. [CrossRef]
15. Flores, H.G.G.; Pugmire, D.L. The growth and evolution of thin oxide films on δ -plutonium surfaces. *IOP Conf. Ser. Mater. Sci. Eng.* **2010**, *9*, 012038. [CrossRef]
16. Dinh, L.N.; Haschke, J.M.; Saw, C.K.; Allen, P.G.; McLean, W. Pu_2O_3 and the plutonium hydriding process. *J. Nucl. Mater.* **2011**, *408*, 171–175. Available online: <https://www.sciencedirect.com/science/article/pii/S0022311510007178> (accessed on 12 October 2022). [CrossRef]
17. Ravat, B.; Jolly, L.; Oudot, B.; Fabas, A.; Guerault, H.; Popa, I.; Delaunay, F. New insight into δ -Pu alloy oxidation kinetics highlighted by using in-situ X-ray diffraction coupled with an original Rietveld refinement method. *Corros. Sci.* **2018**, *138*, 66–74. Available online: <https://www.sciencedirect.com/science/article/pii/S0010938817321911> (accessed on 12 October 2022). [CrossRef]
18. Wang, L.L.; Wan, M.J.; Ma, J.J.; Jiang, G. Molecular dynamics simulation of $\text{U}_{1-x}\text{Pu}_x\text{O}_2$ thermal expansion. *Acta Phys. Sin. (Chin. Ed.)* **2014**, *63*, 083103. Available online: <https://wulixb.iphy.ac.cn/cn/article/id/58990> (accessed on 12 October 2022). [CrossRef]
19. Xie, A.D.; Meng, D.Q.; Luo, D.L.; Ma, M.Z.; Zhu, Z.H. Effect of external electric field on the excited states of plutonium dihydride. *Acta Phys. Sin. (Chin. Ed.)* **2006**, *55*, 2180–2184. [CrossRef]

20. Atlas, L.M.; Schlehman, G.J.; Readey, D.W. Defects in PuO_{2-x}: Density Measurements at High Temperature. *J. Am. Ceram. Soc.* **1966**, *49*, 624. [CrossRef]
21. Sari, C.; Benedict, U.; Blank, H. A study of the ternary system UO₂-PuO₂-Pu₂O₃. *J. Nucl. Mater.* **1970**, *35*, 267–277. Available online: <https://www.sciencedirect.com/science/article/pii/0022311570902114> (accessed on 12 October 2022). [CrossRef]
22. Zhang, L.; Sun, B.; Song, H.F. First principles study of hydrogen behavior in plutonium oxides. *Chin. J. Comput. Phys.* **2020**, *5*, 595–602. Available online: <https://kns.cnki.net/kcms/detail/detail.aspx?doi=10.19596/j.cnki.1001-246x.8118> (accessed on 12 October 2022).
23. Anderson, G.G.; Palermo, J.J.; Schilling, J.D.; Roth, R.; Heuser, J.; Hultgren, S.J. Intracellular bacterial biofilm-like pods in urinary tract infections. *Science* **2003**, *301*, 105–107. [CrossRef] [PubMed]
24. Skriver, H.L.; Andersen, O.K.; Johansson, B. Calculated Bulk Properties of the Actinide Metals. *Phys. Rev. Lett.* **1978**, *41*, 42–45. Available online: <https://link.aps.org/doi/10.1103/PhysRevLett.41.42> (accessed on 12 October 2022). [CrossRef]
25. Petit, L.; Svane, A.; Szotek, Z.; Temmerman, W.M. First-principles calculations of PuO(2+/-x). *Science* **2003**, *301*, 498–501. [CrossRef] [PubMed]
26. Prodan, I.D.; Scuseria, G.E.; Martin, R.L. Covalency in the actinide dioxides: Systematic study of the electronic properties using screened hybrid density functional theory. *Phys. Rev. B* **2007**, *76*, 033101. Available online: <https://link.aps.org/doi/10.1103/PhysRevB.76.033101> (accessed on 12 October 2022). [CrossRef]
27. Svane, A.; Petit, L.; Szotek, Z.; Temmerman, W.M. Self-interaction-corrected local spin density theory of 5f electron localization in actinides. *Phys. Rev. B* **2007**, *76*, 115116. Available online: <https://link.aps.org/doi/10.1103/PhysRevB.76.115116> (accessed on 12 October 2022). [CrossRef]
28. Prodan, I.D.; Scuseria, G.E.; Sordo, J.A.; Kudin, K.N.; Martin, R.L. Lattice defects and magnetic ordering in plutonium oxides: A hybrid density-functional-theory study of strongly correlated materials. *J. Chem. Phys.* **2005**, *123*, 014703. [CrossRef]
29. Jomard, G.; Amadon, B.; Bottin, F.; Torrent, M. Structural, thermodynamic, and electronic properties of plutonium oxides from first principles. *Phys. Rev. B* **2008**, *78*, 075125. Available online: <https://link.aps.org/doi/10.1103/PhysRevB.78.075125> (accessed on 12 October 2022). [CrossRef]
30. Yang, Y.; Lu, Y.; Zhang, P. Optical properties of PuO₂ and α -Pu₂O₃ by GGA+U+QA studies. *J. Nucl. Mater.* **2014**, *452*, 414–418. Available online: <https://www.sciencedirect.com/science/article/pii/S002231151400347X> (accessed on 12 October 2022). [CrossRef]
31. Shi, H.; Zhang, P. First-principles study of α -Pu₂O₃. *J. Nucl. Mater.* **2012**, *420*, 159–163. Available online: <https://www.sciencedirect.com/science/article/pii/S002231151100818X> (accessed on 12 October 2022). [CrossRef]
32. Lu, Y.; Yang, Y.; Zheng, F.; Zhang, P. Electronic and thermodynamic properties of α -Pu₂O₃. *Phys. Lett. A* **2014**, *378*, 3060–3065. Available online: <https://www.sciencedirect.com/science/article/pii/S0375960114008391> (accessed on 12 October 2022). [CrossRef]
33. Zhang, P.; Wang, B.-T.; Zhao, X.-G. Ground-state properties and high-pressure behavior of plutonium dioxide: Density functional theory calculations. *Phys. Rev. B* **2010**, *82*, 144110. Available online: <https://link.aps.org/doi/10.1103/PhysRevB.82.144110> (accessed on 12 October 2022). [CrossRef]
34. Ao, B.; Qiu, R.; Lu, H.; Chen, P. First-principles DFT+U calculations on the energetics of Ga in Pu, Pu₂O₃ and PuO₂. *Comput. Mater. Sci.* **2016**, *122*, 263–271. Available online: <https://www.sciencedirect.com/science/article/pii/S0927025616302737> (accessed on 12 October 2022). [CrossRef]
35. Ao, B.; Tang, J.; Ye, X.; Tao, R.; Qiu, R. Phase Segregation, Transition, or New Phase Formation of Plutonium Dioxide: The Roles of Transition Metals. *Inorg. Chem.* **2019**, *58*, 4350–4364. [CrossRef] [PubMed]
36. Ao, B.; Lu, H.; Qiu, R.; Ye, X.; Shi, P.; Chen, P.; Wang, X. First-Principles Energetics of Some Nonmetallic Impurity Atoms in Plutonium Dioxide. *J. Phys. Chem. C* **2015**, *119*, 14879–14889. [CrossRef]
37. Atta-Fynn, R.; Ray, A.K. Bulk and (112 $\bar{0}$) surface properties of β -Pu₂O₃: A theoretical study using DFT with exact exchange for correlated electrons. *Chem. Phys. Lett.* **2013**, *583*, 42–48. Available online: <https://www.sciencedirect.com/science/article/pii/S009261413009500> (accessed on 12 October 2022). [CrossRef]
38. Lu, Y.; Yang, Y.; Zhang, P. Charge states of point defects in plutonium oxide: A first-principles study. *J. Alloys. Compds.* **2015**, *649*, 544–552. Available online: <https://www.sciencedirect.com/science/article/pii/S09255838815306174> (accessed on 12 October 2022). [CrossRef]
39. Agarwal, R.; Sen, B.K.; Venugopal, V. Phase diagram analysis of (U,Pu)O_{2-x} sub-system. *J. Nucl. Mater.* **2009**, *385*, 112–116. [CrossRef]
40. Ma, B.L.; Wu, Y.Y.; Guo, Y.H.; Yin, W.; Zhan, Q.; Yang, H.G.; Wang, B.T. Effects of Monovacancy and Divacancies on Hydrogen Solubility, Trapping and Diffusion Behaviors in fcc-Pd by First Principles. *Materials* **2020**, *13*, 4876. [CrossRef]
41. Kresse, G.; Furthmüller, J. Efficient iterative schemes for ab initio total-energy calculations using a plane-wave basis set. *Phys. Rev. B* **1996**, *54*, 11169–11186. Available online: <https://link.aps.org/doi/10.1103/PhysRevB.54.11169> (accessed on 12 October 2022). [CrossRef]
42. Blöchl, P.E. Projector augmented-wave method. *Phys. Rev. B* **1994**, *50*, 17953–17979. [CrossRef] [PubMed]
43. Perdew, J.P.; Burke, K.; Ernzerhof, M. Generalized Gradient Approximation Made Simple. *Phys. Rev. Lett.* **1996**, *77*, 3865–3868. Available online: <https://link.aps.org/doi/10.1103/PhysRevLett.77.3865> (accessed on 12 October 2022). [CrossRef] [PubMed]
44. Dudarev, S.L.; Botton, G.A.; Savrasov, S.Y.; Humphreys, C.J.; Sutton, A.P. Electron-energy-loss spectra and the structural stability of nickel oxide: An LSDA+U study. *Phys. Rev. B* **1998**, *57*, 1505–1509. [CrossRef]

45. Zhang, S.X.; Liu, S.Y.; Yan, D.L.; Yu, Q.; Ren, H.T.; Yu, B.; Li, D.J. First principles study on structural stability and mechanical properties of Ta_{1-x}Hf_xC and Ta_{1-x}Zr_xC solid solutions. *Acta Phys. Sin. (Chin. Ed.)* **2021**, *70*, 117102. Available online: <https://wulixb.iphy.ac.cn/cn/article/id/9e8d0b59-fb1e-45d0-abd6-a9fd0bef7357> (accessed on 12 October 2022). [[CrossRef](#)]
46. Ma, J.-J.; Zhang, C.-B.; Qiu, R.; Zhang, P.; Ao, B.; Wang, B.-T. Pressure-induced structural and electronic phase transitions of uranium trioxide. *Phys. Rev. B* **2021**, *104*, 174103. Available online: <https://link.aps.org/doi/10.1103/PhysRevB.104.174103> (accessed on 12 October 2022). [[CrossRef](#)]
47. Ghosh, P.S.; Arya, A. First-principles study of phase stability, electronic and mechanical properties of plutonium sub-oxides. *Phys. Chem. Chem. Phys.* **2019**, *21*, 16818–16829. [[CrossRef](#)]
48. Huang, S.S.; Ma, J.J.; Lai, K.; Zhang, C.B.; Yin, W.; Qiu, R.Z.; Zhang, P.; Wang, B.T. Point defects stability, hydrogen diffusion, electronic structure, and mechanical properties of defected equiatomic γ (U,Zr) from first-principles. *Materials* **2022**, *15*, 7452. [[CrossRef](#)]